

# An embedding-based distance for temporal graphs

Lorenzo Dall'Amico <sup>a,\*</sup>, Alain Barrat <sup>b,†</sup>, Ciro Cattuto <sup>a,†</sup>

<sup>a</sup>ISI Foundation, Turin, 10126, Italy

<sup>b</sup>Aix-Marseille Univ, Université de Toulon, CNRS, CPT, Marseille 13009, France

\*Corresponding to: [lorenzo.dallamico@isi.it](mailto:lorenzo.dallamico@isi.it)

†Equal contribution

September 4, 2024

## Abstract

Temporal graphs are commonly used to represent time-resolved relations between entities in many natural and artificial systems. Many techniques were devised to investigate the evolution of temporal graphs by comparing their state at different time points. However, quantifying the similarity between temporal graphs as a whole is an open problem. Here, we use embeddings based on time-respecting random walks to introduce a new notion of distance between temporal graphs. This distance is well-defined for pairs of temporal graphs with different numbers of nodes and different time spans. We study the case of a matched pair of graphs, when a known relation exists between their nodes, and the case of unmatched graphs, when such a relation is unavailable and the graphs may be of different sizes. We use empirical and synthetic temporal network data to show that the distance we introduce discriminates graphs with different topological and temporal properties. We provide an efficient implementation of the distance computation suitable for large-scale temporal graphs.

**Keywords:** Network science, Temporal networks, Graph distance, Graph embedding

## Introduction

Graphs are ubiquitous mathematical entities formed by a set of *nodes* and one of *edges* connecting them [1–3]. They can model a wide range of interacting systems, such as social [4, 5], technological [6], spatial [7] and biological networks [8], and owe their popularity to their ability to encode the complex relational structure of these systems. Real-world systems, moreover, often have temporal properties that cannot be encoded in static graphs and call for modeling based on time-resolved network representations, known as *temporal graphs* [9]. Examples of these include transportation [10] and ecological networks [11], human close-range interactions [12–16], collaboration networks [17–19], etc.

Given their ubiquitous use in representing such diverse kinds of systems, it is crucial to be able to compare them. In fact, defining and computing a similarity measure between pairs of graphs [20] underpins many important applications and tasks, including machine learning tasks such as graph classification. However, given the high dimensionality of graphs and their structural complexity, many different notions of *distance* can be devised, capturing different properties of interest. Hence, many definitions of distance for static graphs were introduced, as reviewed in Refs. [21–25]. One of the most straightforward approaches is the *edit distance* [26], which counts the number of elementary changes (edge or node removal or addition) needed to transform one graph into another and only accounts for local information. Approaches that probe the global graph structure are usually based on matrix inversion [27, 28] but generally have a high computational cost and approximations are needed to achieve satisfactory computational performances. The above methods are all designed for comparing pairs of graphs with a known correspondence between nodes, a case we will refer to as *matched* graphs. The more general case of *unmatched* graphs entails defining distances for pairs of graphs for which a mapping between nodes is unavailable, and the graphs may have different numbers of

nodes. In this case, one can either extract and compare a suitable set of chosen graph features, as done in Refs. [29, 30], or leverage the spectral properties of appropriate matrix representations [31–34]. In this case, the computational complexity is also a bottleneck, and approximation heuristics are often required [21].

In the case of temporal graphs, the temporal dimension adds to the complexity of graph comparison. Many of the distance measures mentioned above for static graphs were used to study temporal graphs [35], typically to compare the state of the graph at different points in time and to identify anomalies and change points in the temporal evolution of the graph [36–40]. Here instead, we study the problem of comparing temporal graphs, each taken as a whole. Unlike the snapshot-based methods mentioned above [36–40], we rely on a temporal embedding with a dimensionality that is independent of the temporal span of the graphs, so that we can compare temporal graphs with arbitrary, and different, temporal spans. Few notions of distance were proposed to compare temporal graphs with arbitrary time spans. In particular, the method of Ref. [41] is based on a set of features that can be tailored to a specific research question (similarly to [29] for static graphs). Ref. [42] on the other hand addresses the same problem of temporal graph comparison we tackle here, but it assumes the graphs to be *matched* and it is computationally inefficient (the graph dissimilarity is obtained solving an NP-hard optimization problem and the authors propose an approximation running in  $\mathcal{O}(n^3)$  operations, where  $n$  is the number of graph nodes). Finally, Ref. [43] only considers the *unmatched* case and focuses on a specific property of temporal graphs, namely the comparison of temporal paths statistics, to provide a definition of *dissimilarity*.

Here, we propose a computationally efficient method to compute an actual distance metric between pairs of temporal graphs, considering both the matched and unmatched cases. We build our comparison on top of graph embeddings, leveraging ideas from the local and global approaches mentioned above and encoding differences at the topological and temporal levels. Commented Python code that implements the approach described here is available at [github.com/lorenzodallamico/G-DynaDist](https://github.com/lorenzodallamico/G-DynaDist).

## Temporal graphs definitions

Before delving into the details of our main contribution, we first state some basic definitions.

**Definition 1 (Temporal graph)** *A temporal graph  $\mathcal{G}(\mathcal{V}, \mathcal{E}, \mathcal{W})$  is a tuple  $(\mathcal{V}, \mathcal{E}, \mathcal{W})$ , where  $\mathcal{V}$  is a set of  $n$  nodes,  $\mathcal{E}$  a set of temporal edges between nodes, and  $\mathcal{W}$  a set of edge weights. For a discrete variable  $t$  denoting time, all temporal edges  $e \in \mathcal{E}$  have the form  $e = (i, j, t)$ , representing an interaction between nodes  $i$  and  $j$  at time  $t$  and  $w_e$  indicates the positive weight of edge  $e$ . We say an edge  $(ij)$  is active at time  $t$  if  $(i, j, t) \in \mathcal{E}$ . A node  $i$  is active at time  $t$  if it belongs to an active edge at  $t$ .*

The graph  $\mathcal{G}(\mathcal{V}, \mathcal{E}, \mathcal{W})$  can be represented with a sequence of *weighted adjacency matrices*,  $\{W_t\}_{t=1, \dots, T}$ , where  $T$  is the number of time points. Each of these matrices has size  $n \times n$  and entries  $(W_t)_{ij} = w_{(i,j,t)} > 0$  if  $(i, j, t) \in \mathcal{E}$  and  $(W_t)_{ij} = 0$  otherwise. In the following, we will refer to these matrices as “snapshots” of the temporal graph at given times and to  $T$  as the number of snapshots [44]. In a more general description of temporal networks, each interaction may be represented with a tuple  $(i, j, t, \tau)$  where  $\tau \in \mathbb{R}^+$  is an *interaction duration*. We adopt the former notation because it is simpler to handle in the following. The two notations are completely interchangeable whenever the time is discrete and a finite temporal resolution  $t_{\text{res}}$  is set. In fact, all contacts with a duration within  $t_{\text{res}}$  are considered to be instantaneous, and  $(i, j, t, \tau)$  can be represented by a set of interactions of unitary duration:  $\{(i, j, t + \delta)\}_{\delta \in \{0, \dots, \tau-1\}}$ . For this reason, Definition 1 is sufficiently general, as it can also describe interactions lasting more than one temporal unit. For increasing values of  $t_{\text{res}}$ , the temporal graph gets progressively more aggregated and loses information on the temporal ordering of contacts within  $t_{\text{res}}$ , but partial information can be retained with edge weights expressing the fraction of  $t_{\text{res}}$  in which the edge was active.

Let us now introduce the concept of *matched* and *unmatched* graphs.

**Definition 2 (Matched graphs)** *Let  $\mathcal{G}_1(\mathcal{V}_1, \mathcal{E}_1, \mathcal{W}_1)$  and  $\mathcal{G}_2(\mathcal{V}_2, \mathcal{E}_2, \mathcal{W}_2)$  be two temporal graphs with  $n_1$  and  $n_2$  nodes, respectively. We say that  $\mathcal{G}_1$  and  $\mathcal{G}_2$  are matched if  $n_1 = n_2$  and there exists a known bijective function  $\pi : \mathcal{V}_1 \rightarrow \mathcal{V}_2$  that maps each node of  $\mathcal{G}_1$  to a node of  $\mathcal{G}_2$ . The two graphs are otherwise said to be unmatched.*

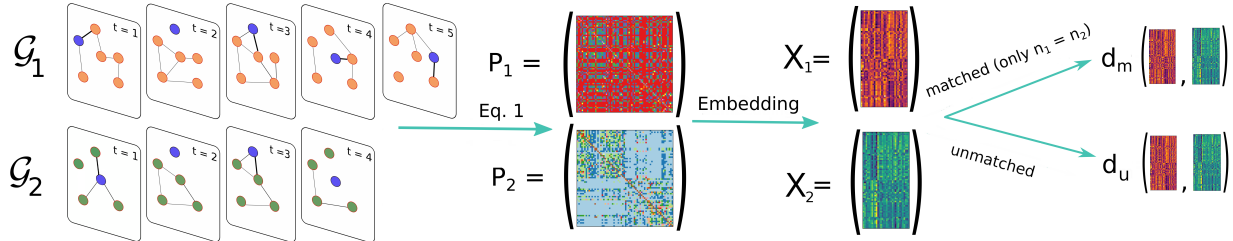


Figure 1: **Distance computation between two temporal graphs.** The inputs to the distance function are two temporal graphs  $\mathcal{G}_1$  (top, orange nodes) and  $\mathcal{G}_2$  (bottom, green nodes), generally with a different number of snapshots ( $T_1 = 5, T_2 = 4$ , in the example) and a different number of nodes  $n$  (here  $n_1 = 6, n_2 = 5$ ). Each graph is represented as a matrix  $P \in \mathbb{R}^{n \times n}$ , according to (1), with entry  $(ij)$  encoding the probability that a random walker goes from  $i$  to  $j$  following a time-respecting path (the walker’s position at each time point is indicated in blue). The matrices  $P_1, P_2$  are then embedded using the EDRep algorithm, mapping them to  $X_1 \in \mathbb{R}^{n_1 \times d}$  and  $X_2 \in \mathbb{R}^{n_2 \times d}$ . Finally, the matched – (3) – and unmatched – (4) – distances are calculated. Notice that a necessary condition to compute  $d_m$  is that  $n_1 = n_2$ .

When two graphs have the same size, *i.e.*, the same number of nodes, there are always many possible mappings  $\pi$  between their nodes, but for the *matched* approach to be valuable, a known mapping associated with an external notion of node identity across the two graphs is necessary (e.g., nodes corresponding to the same persons in two temporal social networks). An implicit consequence of Definition 2 is that all graph pairs with a different number of nodes are considered to be *unmatched*. We now state the requirements for our distance measure and illustrate our main result.

## Main result

In the following, we define two types of distance functions:  $d_m, d_u$  between matched and unmatched graphs, respectively. The inputs to these functions are two temporal graphs,  $\mathcal{G}_1$  and  $\mathcal{G}_2$ , with potentially different numbers of time points (snapshots)  $T_1$  and  $T_2$ . In both cases, the distances should fulfill the following standard requirements [45]: i) non-negativity; ii) separation axiom; iii) symmetry; iv) triangle inequality. In addition, both distances should be able by design to detect differences induced by the permutation of time indices. The matched distance should also differentiate between temporal networks differing only by a permutation of node indices, while the unmatched one should be invariant under such transformation.

Our proposed distances are computed in two steps: i) we generate a temporal graph embedding, given by a matrix of size  $(n \times d)$  (with  $d$  independent of  $T$ ), that encodes relevant topological and temporal properties by leveraging time-respecting random walks on the temporal network; ii) we define the distance in the embedded space, treating separately the matched and the unmatched cases. The distance computation pipeline is illustrated in Fig. 1. The steps outlined above are described in detail in the next two Sections titled **Temporal graph embedding** and **Defining an embedding-based distance**.

### Temporal graph embedding

Graphs are rich data representations, making it challenging to define simple mathematical operations to manipulate them. Graph embeddings provide an interesting avenue for doing so, as they yield a representation in vector space that preserves some of the graphs’ relevant properties [46–49]. In the case of temporal graphs, the additional challenge of dealing with their temporal dimension has been tackled in many different ways: Ref. [50] represents time as an additional dimension of an adjacency tensor; in evolutionary spectral clustering [51–55], a different embedding is obtained for each snapshot, and smoothness conditions are implemented on their temporal evolution; more recent work [56–58] introduced approaches based on time-respecting random walks, which encode temporal properties relevant for dynamical processes occurring on temporal graphs; Refs. [39, 40] also build one embedding per snapshot for studying the graph evolution and comparing different time points. The authors argue that a graph comparison metric should depend on the whole graph structure and thus define graph instead of node embeddings.

With a similar approach to [58], we start from time-respecting random walks to generate temporal graph embeddings, which we use to define a distance based on global temporal graph properties. The embeddings are obtained as the solution to an optimization problem. We define a loss function whose argument is a transition matrix  $P$  that is the limiting distribution of time-respecting random walks over the temporal graph  $\mathcal{G}$  to be embedded.  $T$  being the number of snapshots of  $\mathcal{G}$ , we consider an ensemble of random walks of length  $\ell$  drawn uniformly at random between 1 and  $T$ , and starting from a randomly chosen node at time  $t = T - \ell + 1$ ; at each time step, the walker, situated, e.g., on node  $i$ , can either move to a random neighbor of  $i$  in the snapshot at time  $t$  or stay in place on  $i$ ; if the walker is situated on a node that is not active at time  $t$ , *i.e.*, which has no neighbors in this snapshot, the walker stays in place with probability one. The graph snapshots on the left of Fig. 1 show examples of such time-respecting random walks on the input graphs.

Specifically, given a temporal graph  $\mathcal{G}$ , with  $W_t$  the snapshot adjacency matrices at times  $t = 1, \dots, T$ , we define for each snapshot  $\hat{L}_t = (D_t + I_n)^{-1}(W_t + I_n)$ , where  $D_t$  is the degree matrix  $D_t = \text{diag}(W_t \mathbf{1}_n)$  of the snapshot,  $I_n$  is the identity matrix of size  $n \times n$ , and  $\mathbf{1}_n$  is the  $n$ -sized unity vector. We then define the matrix  $P$  as

$$P = \frac{1}{T} \sum_{\tau=1}^T \hat{L}_\tau \hat{L}_{\tau+1} \cdots \hat{L}_T, \quad (1)$$

The matrices  $\hat{L}_t$  and  $P$  are sometimes referred to as *temporal transition matrix* and *global transition matrix*, respectively. The properties of time-respecting random walks depend on several properties of the temporal graph, that may include, for instance, the presence of a non-Markovian behavior, and of a broad distribution of the edge activity and inter-event durations [59]. The limiting probability matrix  $P$  of time respecting random walks encodes the aforementioned properties and it is sensitive to the permutation of time indices. We remark that the random walks we use can be of arbitrary length. Hence, the matrix  $P$  is, in principle, sensitive to all time scales of the temporal graph at hand.

Given the above probability matrix  $P$  and a chosen embedding dimensionality  $d$ , we now generate, for each node  $i$  of  $\mathcal{G}$ , a unitary node embedding vector  $\mathbf{x}_i \in \mathbb{R}^d$ . To this end, we define  $X \in \mathbb{R}^{n \times d}$  as a matrix where each row represents an embedding vector. We then express the loss function as:

$$\begin{aligned} \mathcal{L}_P(X) &= - \sum_{i,j \in \mathcal{V}} \left[ P_{ij} \log Q_{ij}(X) - \frac{\mathbf{x}_i^T \mathbf{x}_j}{n} \right], \quad (2) \\ Q_{ij}(X) &= \frac{e^{\mathbf{x}_i^T \mathbf{x}_j}}{\sum_{k \in \mathcal{V}} e^{\mathbf{x}_i^T \mathbf{x}_k}} := \frac{e^{\mathbf{x}_i^T \mathbf{x}_j}}{Z_i}. \end{aligned}$$

This loss function is the sum of the cross entropies between the distributions in the rows of  $P$  and the variational distributions in the rows of  $Q(X)$ , with the addition of a regularization term. Since  $Z_i$  is computed in  $\mathcal{O}(n)$  operations for each  $i$ , the function  $\mathcal{L}_P$  requires  $\mathcal{O}(n^2)$  operations to be computed. We adopt the recently proposed **EDRep** algorithm [60] that introduces an efficient approximation of  $Z_i$ , optimizing  $\mathcal{L}_P$  in  $\mathcal{O}(n)$  operations. For further details, we refer the reader to the **Methods** section.

The matrix  $X$  obtained by optimizing  $\mathcal{L}_P$  defines the embedding of the temporal graph  $\mathcal{G}$ . In the following, we show how to leverage this embedding to define a distance between temporal graphs.

## Defining an embedding-based distance

We want to define a distance between temporal graph embeddings satisfying the requirements stated above. Notice that the embedding vectors  $\mathbf{x}$  are defined up to an orthogonal transformation applied to the rows of  $X$ . In fact, suppose  $R \in \mathbb{R}^{d \times d}$  is an orthogonal matrix, and  $\tilde{\mathbf{x}}_i = R \mathbf{x}_i$ , then  $\mathbf{x}_i^T \mathbf{x}_j = \tilde{\mathbf{x}}_i^T \tilde{\mathbf{x}}_j$  and the loss function of (2) is  $\mathcal{L}_P(\tilde{X}) = \mathcal{L}_P(X)$ . Hence, our distance must be invariant under orthogonal transformations. Moreover, as discussed above, the distance for unmatched graphs must also be invariant with respect to node permutations.

Given these requirements, we now discuss separately our choices for the the matched and unmatched cases. In the **Empirical evaluation** section, we show the ability of our distances to discriminate temporal graph classes that differ for topological or temporal properties.

### Distance for matched graphs

Let  $X_1$  and  $X_2 \in \mathbb{R}^{n \times d}$  be the embedding matrices of two matched temporal graphs  $\mathcal{G}_1$  and  $\mathcal{G}_2$ . To satisfy the invariance requirements discussed above, rather than defining our distance directly in terms of the matrices  $X_1$  and  $X_2$ , we use the auxiliary matrices  $M_{X_1} = X_1 X_1^T$  and  $M_{X_2} = X_2 X_2^T$  of size  $n \times n$ . These matrices are by construction invariant with respect to orthogonal transformations of the embedding space and encode the global structure of the corresponding temporal graphs, as the embeddings are generated using the complete temporal network information. We define the distance  $d_m$  between matched temporal graphs as:

$$d_m(\mathcal{G}_1, \mathcal{G}_2) := \|M_{X_1} - M_{X_2}\|_F ,$$

where  $\|\cdot\|_F$  is the Frobenius norm. Each matrix  $M$  encodes the similarity in the embedding space between all pairs of nodes of the corresponding temporal graph, and  $d_m$  quantifies thus the difference between these similarity patterns. In the **Methods** section, we show that we do not need to actually compute the large ( $n \times n$ )  $M_{X_1}$  and  $M_{X_2}$  matrices, but that the distance can be computed using the generally smaller  $d \times d$  matrices as follows:

$$d_m(\mathcal{G}_1, \mathcal{G}_2) = \sqrt{\|X_1^T X_1\|_F^2 + \|X_2^T X_2\|_F^2 - 2\|X_1^T X_2\|_F^2} , \quad (3)$$

We can easily verify that  $d_m$  is a distance, as it satisfies all the requirements mentioned above and is generally not invariant under the permutation of node indices. Notice that, even if  $d_m$  can be computed for any pair of graphs with the same size, this distance is only meaningful for matched graphs (i.e., with known matching). In (3), the term  $X_1^T X_2$  implies that  $X_1$  and  $X_2$  have the same size and that their rows are ordered according to the same node index.

### Distance for unmatched graphs

In the case of *unmatched* graphs, there is no correspondence between nodes, and the distance, as we discussed, should also be invariant with respect to node permutations. We therefore define the distance between unmatched graphs using auxiliary vectors. Specifically, we denote with  $\lambda(A)$  the vector of ordered eigenvalues of a matrix  $A$  and define our distance between two *unmatched* temporal graphs as

$$d_u(\mathcal{G}_1, \mathcal{G}_2) = \left\| \lambda \left( \frac{X_1^T X_1}{n_1} \right) - \lambda \left( \frac{X_2^T X_2}{n_2} \right) \right\|_2 , \quad (4)$$

where  $X_1$  and  $X_2$  are, as before, the embeddings matrices of the two graphs, with sizes  $n_1 = |\mathcal{V}_1|$  and  $n_2 = |\mathcal{V}_2|$ . The normalization of the covariance matrices  $X_1^T X_1$  and  $X_2^T X_2$  is chosen so that their eigenvalues are independent from the graph size.

In the **Methods** section we show that the covariance matrices  $X_1^T X_1$  and  $X_2^T X_2$  (of size  $d \times d$ ) are indeed an appropriate argument of the distance function  $d_u$ , since they are independent of the ordering of the nodes and any other orthogonal transformation applied to the columns of  $X_1$  and  $X_2$ . However, a direct comparison of the entries of  $X_1^T X_1$  and  $X_2^T X_2$  would require a one-to-one correspondence between the embedding dimensions, i.e., the columns of  $X_1$  and  $X_2$ . This mapping is unavailable because the **EDRep** algorithm, like most vector-space embedding techniques, makes no guarantees on the correspondence between the dimensions of the embedding vectors corresponding to different graphs. To tackle this issue, we thus compare the spectra, which are invariant with respect to orthogonal transformations of the rows of the embedding matrices. This choice takes inspiration from spectral distance definitions for static graphs, such as Ref. [33], in which graphs are compared by computing the distance between the ordered sets of the eigenvalues of their matrix representations (e.g., adjacency, Laplacian, non-backtracking, etc.)

### Computational complexity

As discussed in the **Methods** section, the computational complexity of the embedding step is  $\mathcal{O}(nd^2 + d \cdot \min(n^2, E))$ , where  $E = \sum_t |\mathcal{E}_t|$  is the total number of temporal edges. On top of this, the distance  $d_m$  is then obtained with  $\mathcal{O}(nd^2 + d^2)$  additional operations, while  $d_u$  requires  $\mathcal{O}(nd^2 + d^3)$  additional operations.

## Empirical evaluation

We now evaluate the distance definitions we introduced, particularly with respect to their sensitivity to important topological and temporal properties of empirical temporal graphs. We carry out three kinds of evaluation tests using both synthetic and empirical temporal graph data. We use, in particular, empirical data shared by the **SocioPatterns** collaboration ([sociopatterns.org](http://sociopatterns.org)) describing time-resolved, close-range proximity interactions of humans and animals in a variety of real-world environments (see Table 1 of the **Methods** section). These data are known to exhibit rich multi-scale network structures, complex temporal activity patterns, correlations between these two, and other complex network features [61]. Hence, they provide a natural benchmark to assess the sensitivity of our distance definitions to several specific properties of real-world temporal graphs. It is important to note that these data sets are by no means an exhaustive sample of temporal networks. However, our goal here is to show that the distances we introduce are sensitive to complex properties of temporal networks that we know are present in these particular data sets. Therefore, the evaluations we outline below do not depend on testing our distances on a comprehensive set of temporal networks but rather rely on making tests using data that are well understood, have been and are widely used by the scientific community and are known to exhibit many important properties of temporal graph data.

1. *Discriminating between classes of temporal graphs.* We consider topologically different synthetic temporal graphs of different sizes and we cluster them using our temporal graph distance  $d_u$ , checking how well the clusters we find match the known classes of the generative method we used, irrespective of graph size. We then carry out the same test using empirical graphs on human proximity in school settings.
2. *Detecting partial node relabeling.* We consider a synthetic temporal graph, select a fraction of its nodes, shuffle their indices and compute the distance  $d_m$  between the original and the re-labeled graphs. We investigate the behavior of the distance  $d_m$  as a function of the fraction of re-labeled nodes.
3. *Discriminating between temporal graph randomizations.* We use the empirical data to elucidate which of the many properties of real temporal graphs are discriminated by the distances we introduced. We proceed as follows: given an empirical temporal graph, we apply to it a set of randomization operations, where each operation is designed to preserve specific properties of the original data (e.g., the activity time series of each node). We then attempt to discriminate the randomized temporal graphs from one another using our distance definitions and quantify the performance of such discrimination tasks. We test both  $d_m$  and  $d_u$ ; however, by design, this evaluation strategy compares temporal graphs with the same number of nodes.

### Discriminating between classes of temporal graphs

To test the ability of our model to distinguish topological network features, we proceed as follows. We consider four random generative models for static graphs and generate 250 instances from each model with size uniformly distributed between  $n = 200$  and  $n = 1800$  and constant average degree. The models we use are: i) the Erdős-Renyi (ER) model [62]; ii) the stochastic block model (SBM), capable of generating graphs with a known community structure [63]; iii) the configuration model (CM), yielding graphs with an arbitrary degree distribution [64]; iv) the geometric model (GM), which generates edges based on proximity in a latent space [65]. Unlike the first three, the latter model yields graphs with a high clustering coefficient. Details on these generative models are provided in the **Methods** section. We then turn these graphs into temporal graphs by assigning an activity time series to each edge of the static graph, *i.e.* a set of timestamps at which that edge is active. To do this, we copy the activity time series of a randomly chosen edge of an empirical temporal graph, namely the *Conference* data set, which has the largest number of nodes among the empirical data sets we use. Details on the properties of this data set are given in Table 1. We then deploy our distance definition  $d_u$  to compute a pairwise distance matrix between all these temporal graphs and use this matrix as an input for an unsupervised clustering algorithm to label each graph. The unsupervised clustering algorithm only takes the distance matrix and the number of clusters  $k$  (here  $k = 4$ ) as inputs. Here, we first perform a spectral embedding of the distance matrix between graph pairs using non-negative matrix factorization (NMF) [66] extracting  $k$  non-negative components and then applying the k-means clustering algorithm with



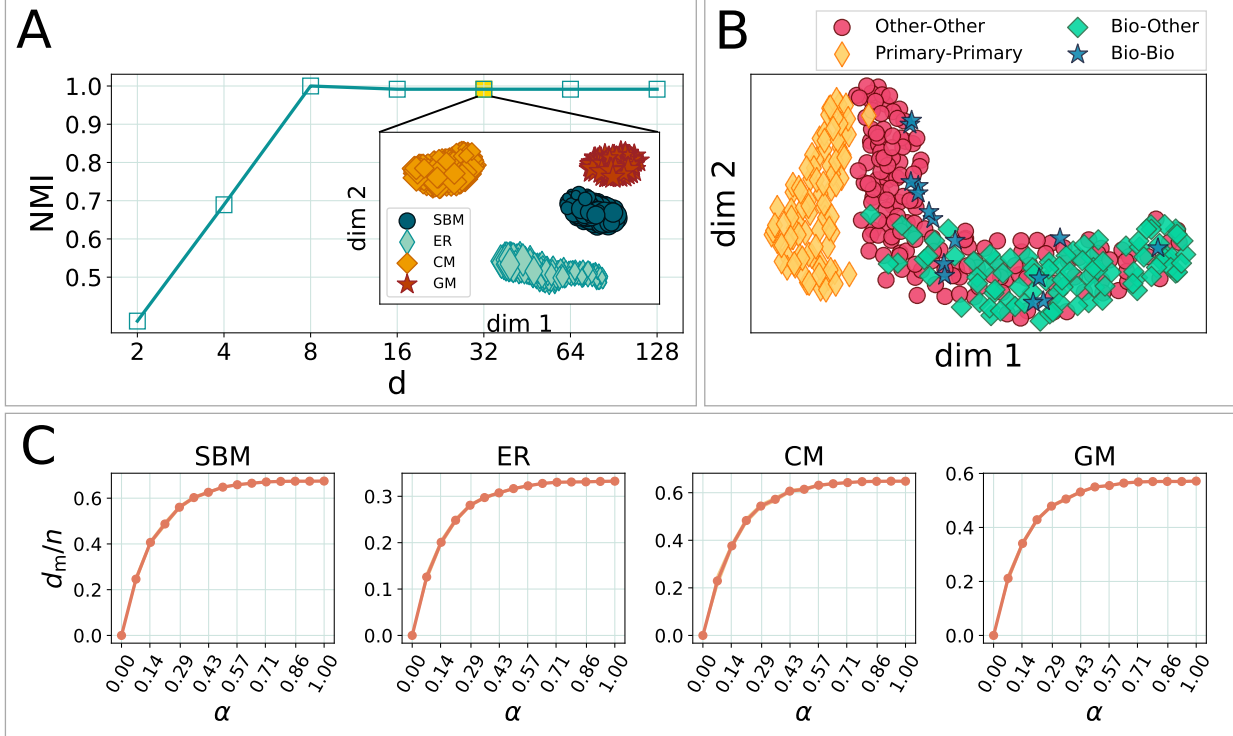


Figure 2: **Validation of the distances on graphs of varying size.** *Panel A:* Accuracy of the distance-based clustering against the ground truth classes in terms of normalized mutual information (NMI) as a function of the embedding dimensionality  $d$  used in the embedding step shown in Figure 1. The clustering task consists in recognizing four synthetic temporal graph classes with an unsupervised algorithm based on the distance  $d_u$ . The synthetic graphs classes are obtained by generating a graph from either of four models (stochastic block model (SBM), configuration model (CM), Erdős-Renyi (ER), and geometric model (GM)) with constant degree equal to 4.8, and the temporal component is obtained by sampling the edge activity of an empirical graph, as detailed in the main text. *Inset of panel A:* Scatter plot of UMAP dimensionality reduction in two dimensions of the vectors  $\lambda$  appearing in the definition of  $d_u$  given in (4), with here  $d = 32$ . Each point refers to a temporal graph; the color and marker code refer to the generative model of its static component, while the marker size is proportional to the number of nodes. *Panel B:* Each point is the 2-dimensional UMAP embedding of the vector  $\lambda$  of the temporal graph obtained selecting two classes and a day of interaction for all possible  $(c_2, c_2, \text{day})$  triplets in the `SocioPatterns` data sets describing proximity temporal graphs in schools. The color and marker code are assigned according to the class labels: the primary school classes form a group on their own and the other three groups (*Other-Other*, *Bio-Other*, *Bio-Bio*) belong to the high school data sets, where *Bio* are the biology classes, and *Other* the remaining ones. In all cases, we use a temporal resolution equal to 10 minutes to create the temporal graphs from the `SocioPatterns` data. *Panel C:* normalized matched distance between a temporal graph and itself upon partial node re-labeling, as a function of the fraction  $\alpha$  of re-labeled nodes. Each plot considers one of the generative models used in panel A, with the same nomenclature used for the title. The – barely visible – shadow line is the standard deviation of the distance value across 25 randomizations of the partial re-labeling.

$k$  classes [67]. We note that successively embedding and clustering is a standard approach, and using NMF is most suited here since the distance matrix is non-negative. Finally, we compare the original temporal graph labels (i.e., the classes of our generative model) with the partition labels yielded by unsupervised clustering based on our distances: we quantify the match between the true partition and the inferred one using the normalized mutual information (NMI), which yields a performance metric ranging between 0 (random guess) and 1 (perfect reconstruction).

Figure 2A shows the normalized mutual information (NMI) between the known temporal graph classes (associated with the four generative models) and the discovered cluster labels, as a function of the embedding dimension  $d$ . The discrimination performance is low for small values of  $d$ , but for  $d \gtrsim 8$  the accuracy is high and becomes insensitive to the specific value of  $d$ . The inset in Figure 2A shows the output of UMAP algorithm [68] in two dimensions when applied to the vectors  $\lambda \in \mathbb{R}^{32}$  used in the distance  $d_u$ . Each symbol corresponds to one temporal graph, the color and marker shape indicate its generative model and the marker size is proportional to the number of graph nodes. We observe that graph size does not appear to affect

distances systematically and that the  $\lambda$  vectors used by the distance  $d_u$  allow us to discriminate all four generative models. Indeed, we have verified that the distances  $d_u$  between the graphs and the distances between their respective UMAP embedded vectors are strongly correlated, with a highly significant Spearman correlation coefficient of  $\sim 0.92$ .

We now carry out a test using the **SocioPatterns** empirical data sets describing time-resolved, close-range proximity interactions in schools over multiple days. These data sets are *Primary school*, *High school 1*, *High school 2*, *High school 3*. In these graphs, the nodes can be grouped according to school classes. In the primary school data set, there are ten classes, subdivided into two sections and five grades. In the high school data sets, the classes are defined by the main topics studied by the students: these topics can be maths and physics, physics and chemistry, or biology. The 2011 data set is composed of three classes on physics and chemistry; the 2012 data set has two additional classes on physics and maths; the 2013 data set contains another physics and maths class and three biology classes. The metadata grouping nodes into classes are provided alongside the temporal networks data sets. We then assign one label to each class: the label is *Primary* for all primary school classes, while for the high school data sets, we only make the distinction between biology classes, labeled as *Bio*, and all others, labeled as *Other*.

Given a pair of classes  $c_1, c_2$  from the same data set, we construct triplets  $(c_1, c_2, \text{day})$  inducing sub-temporal graphs formed by all the interactions on that day between the students of the two classes. For each sub-temporal graph, we compute the vector  $\lambda$  of Equation (4) and further decrease its dimensionality to  $d = 2$  using UMAP. We find that the Spearman correlation between the distances  $d_u$  and the distances between the UMAP embedding vectors is very high, namely equals 0.88. Finally, we plot the resulting embedding in Fig. 2B, in which each point corresponds to a triplet. The color and marker coding denote the types of the two interacting classes. The plot shows that the distance can disentangle the networks formed from primary school data from those containing high school data. Moreover, a less neat but still visible distinction exists in the embeddings of  $(\text{Bio-Other})$  with respect to the other triplets, likely because biology students spent more time in the labs and had different interaction patterns. This result confirms the ability of our distance to capture information on the temporal graph at multiple levels.

## Detecting partial node relabeling

One required property for matched distance is to distinguish between graphs that differ only upon a node re-labeling. We work with the synthetic temporal graphs defined in section **Discriminating between classes of temporal graphs** to evaluate our distance in accomplishing this task. For each random graph model, we i) generate an instance of the random graph with  $n = 1000$  nodes; ii) randomly select a fraction  $\alpha$  of nodes and shuffle their labels; iii) compute the distance between the original graph and the partially re-labeled one. This is repeated for 25 different realizations of the partial re-labeling. Figure 2C shows the distance  $d_m$  (rescaled by the graph size) as a function of  $\alpha$ . The plots confirm for all the considered generative models that the distance depends on partial node re-labeling, with a positive distance as soon as  $\alpha > 0$ , and increases with the fraction  $\alpha$  of relabeled nodes. Notably, the plot suggests a high discriminative power even for small  $\alpha$  values, as the distance increases rapidly with  $\alpha$ .

## Discriminating between temporal graph randomizations

Let us now consider 9 empirical **SocioPatterns** data sets, whose basic properties are summarized in Table 1 of the **Methods** section. Following Ref. [69], we select 6 types of randomization operations  $R_i$  ( $i = 1, \dots, 6$ ), described in detail in the **Methods** section. In all cases, we preserve the number of nodes and the number of snapshots of the original temporal graph. These six randomizations are chosen because they allow us to inspect relevant temporal graph properties, including the interaction duration distribution, the node activation time series, the strength distribution in the aggregated graph, or the presence of a community structure. We can thus investigate graph properties both at the topological and temporal levels.

To quantify the discriminative performance of our temporal graph distance, we proceed as follows, separately for each empirical temporal graph: given the empirical temporal graph and a pair of randomization operations  $(R_i, R_j)$ , we generate a set of 250 realizations using  $R_i$ , labeled as 0, and a set of 250 realizations using  $R_j$ , labeled as 1, for a total of 500 temporal graphs. We then compute the matrix of distances between these 500 graphs and use it to cluster them in 2 clusters, following the same procedure used for Fig. 2A.



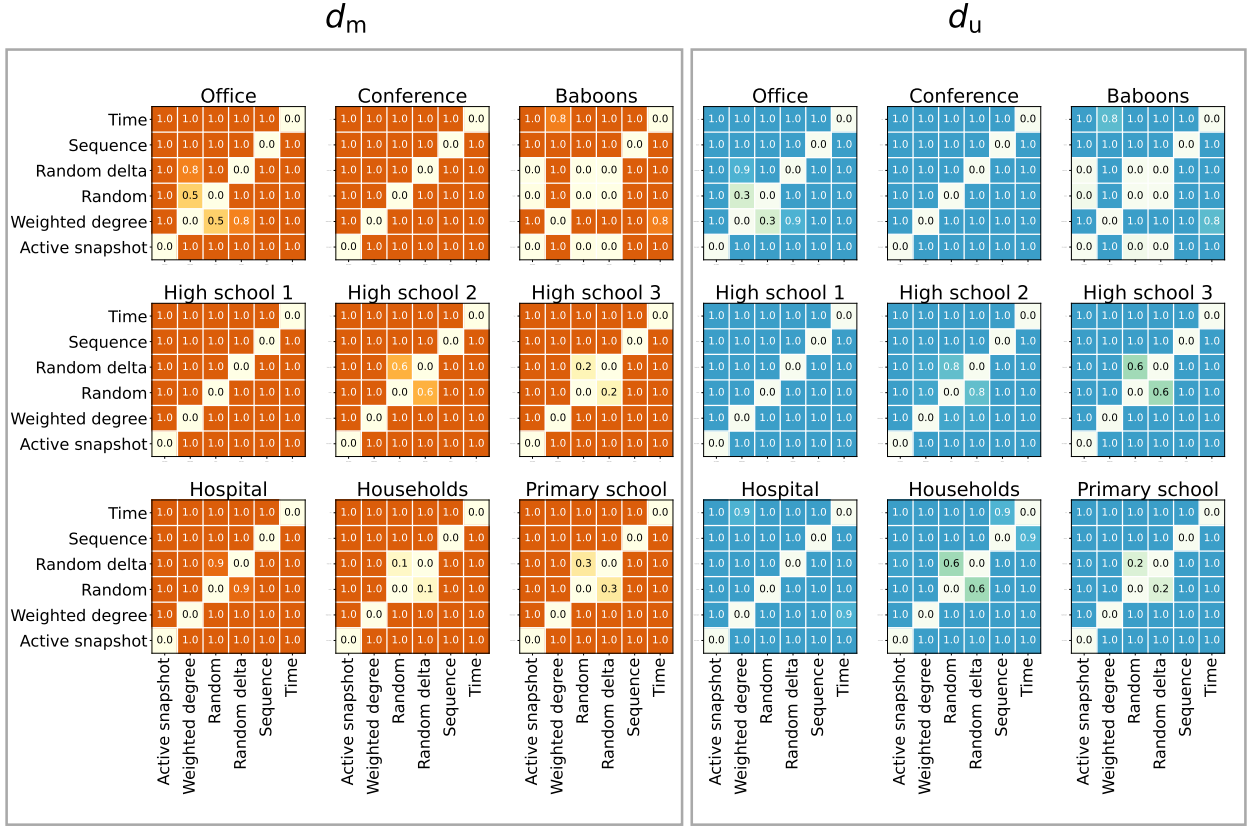


Figure 3: **Distance-based graph clustering for ensembles of temporal graphs generated according to different randomization techniques.** *Left panel:* results for the matched distance  $d_m$  of (3). *Right panel:* results for the unmatched distance  $d_u$  of (4). Within each panel, each matrix corresponds to one of the 9 **SocioPatterns** temporal graphs described in Table 1. The rows and columns of each matrix correspond to the same set of 6 randomization techniques we used, described in the **Methods** sections. Each input graph is represented as a sequence of temporal edges  $(i, j, t)$  as per Definition 1. The randomizations act on the temporal edges as follows. *Random:* preserves the number of temporal edges and randomizes the node and time indices; *Random delta:* preserves the number of temporal edges and interaction duration distribution; *Active snapshot:* preserves the number of edges at each time-step and the times at which each node is *active*, *i.e.*, at which it has at least one neighbor. *Time:* preserves the aggregated weighted graph structure, *i.e.*, the number of times each edge is active in the temporal graph; *Sequence;* preserves each snapshot’s adjacency matrix and randomizes the order in which they appear; *Weighted degree:* preserves the total number of temporal edges involving each node. For each pair of randomizations, we infer the randomization method of each temporal graph via an unsupervised distance-based clustering algorithm, and we compare the inferred randomization method with the known true one. Each matrix entry reports (value and color coding) the accuracy of the inferred labels (randomization methods), quantified as the normalized mutual information (NMI) between the inferred and true labels.

Figure 3 reports the NMI values between the real labels and the unsupervised algorithm result for each pair of randomizations  $(R_i, R_j)$ , and for both the matched distance  $d_m$  (left panel) and the unmatched distance  $d_u$  (right panel). Within each panel, each matrix refers to one empirical temporal graph, and its entries are the NMI values described above. A high NMI entry indicates that our distance discriminates well the temporal graphs generated according to the two randomization procedures in the corresponding row and column of the matrix entry, *i.e.*, that the distance is sensitive to the properties preserved by either  $R_i$  or  $R_j$ . Low NMI values may either correspond to an inability of the distance to capture those properties or simply reflect that the empirical temporal graph is statistically random as far as those properties are concerned, as observed in particular for several pairs of randomizations in the *Baboons* data set. Thus, it is enough to find one empirical data set for which the distance can distinguish between a pair of randomizations to conclude that the distance is indeed sensitive to the corresponding graph properties.

## Conclusions

We introduced a novel definition of distance between pairs of temporal graphs. This definition entails two steps. First, the temporal graphs are embedded in Euclidean space, and then a distance is defined in embedded space. For the first step, we use an embedding based on time-respecting random walks over the temporal graph. Such walks are known to depend on and to encode important structural and temporal properties of time-varying graphs [9, 43, 58, 59, 70]. For the second step, we proposed two possibilities for the distance definition: if a mapping is known between the nodes of the graphs to be compared, we consider a distance definition that leverages such mapping; in the more general case, when such a mapping is unavailable, we put forward a definition that makes it possible to compare graphs with arbitrarily different sizes (numbers of nodes). In both cases, since the size of the embedding matrix we use does not depend on the graph’s temporal span, it is possible to embed temporal graphs with different durations in the same embedding space and thus compute a distance between them. The evaluation of our approach on both synthetic and empirical data shows that the proposed distance is sensitive to structural differences (e.g., degree distribution, clustering coefficient, or presence of communities) as well as to temporal differences (e.g., burstiness or node activity patterns) of the temporal graphs being compared.

The methodology we developed is very general and customizable, as several alternative choices are possible for both steps of our approach, namely the chosen embedding method and distance. The specific choices we study here are motivated by two considerations: i) a theoretical one, given the importance of time-respecting random walks in encoding information on temporal graphs, and thus in generating distributed representations of temporal graphs [9, 58, 59, 70]; ii) a numerical one, which led us to choose the **EDRep** algorithm of Ref. [60] because of its efficiency and scalability. Our evaluation results support these choices *a posteriori*.

Some limitations of our approach are worth mentioning. First, the part of our evaluation based on empirical data focused on a limited set of temporal graphs, namely temporal networks describing the close-range proximity of humans. However, these temporal graphs are known to feature a broad variety of representative structural and temporal features, such as time-varying community structures, burstiness of edge activity, fat-tailed distributions of interaction durations, and more [13, 15]. Second, we only considered the cases of fully matched graphs (a bijective relation between nodes) or no known matching. An interesting intermediate situation would be partially matched graphs, in which only a subset of nodes are matched across the two graphs. Tackling this challenging case would yield an interesting extension of our work. Finally, our unmatched distance allows us to compare graphs with sizes (number of nodes) that potentially differ even by orders of magnitude. Even if our definition can deal with such extreme cases, we believe that this kind of comparison calls for a more profound question on what it means to compare entities that differ so much. This case might require tailored definitions of distance that leverage domain-specific knowledge.

Defining a distance between temporal graphs opens the door to a wealth of potential applications, of which our evaluation only offers possible examples. On the one hand, such a distance can support data analysis of temporal graph data by extending the procedure of Figure 3 to a richer set of randomizations [50]. Indeed, as discussed, the inability to distinguish pairs of randomizations of a given temporal graph can be regarded as an invariance property of the graph itself. On the other hand, computing a distance between graphs can provide a crucial tool for the validation of generative models: the validation of generative models is often limited to comparing a set of statistical properties [41], while our distance definition enables us to carry out a comparison at the global level. In addition, our distance could underpin the very process of generating synthetic temporal graphs by enabling approaches such as *GANS* [71] that depend on a global distance and have proved extremely powerful in generating realistic data [72, 73]. In particular, generating synthetic human proximity data with realistic topological and temporal properties could be used to better simulate infectious disease spread and other phenomena of interest for public health research [74–79]. Finally, we know that empirical (temporal) graphs are hard to anonymize [78, 80, 81]. To minimize the risk of node re-identification, performing some perturbation operations on the graph might be necessary before making it publicly available. However, such operations risk destroying essential patterns and information of empirical data. The distance we introduced could help tackle the trade-offs between re-identification risk and information loss by better quantifying the latter.

# Methods

## The EDRep algorithm

The EDRep algorithm [60] was recently proposed to efficiently generate embeddings given a probability matrix encoding the affinity between the embedded items. This is done by optimizing the cost function of (2) under the constraint  $\|\mathbf{x}_i\| = 1$  and obtaining a low-dimensional representation of the information encoded in the matrix  $P$ . A known problem of this type of cost function is the computational complexity because the normalization constants  $Z_i = \sum_{k \in \mathcal{V}} e^{\mathbf{x}_i^T \mathbf{x}_k}$  require  $\mathcal{O}(n^2)$  to be calculated. However, Ref. [60] describes an efficient way to estimate all the  $Z_i$  values in  $\mathcal{O}(n)$ . This is accomplished by first subdividing the nodes into  $q$  groups based on the embedding matrix  $X$ . Here  $q$  is a parameter of the algorithm, and larger  $q$  values generally lead to a higher accuracy, but very good results are obtained already for  $q = 1$ . Second, for each  $a = 1, \dots, q$ , one computes the mean  $\boldsymbol{\mu}_a$  and the covariance matrix  $\Omega_a$  of the set of embedding vectors of the nodes in group  $a$ . Denoting the number of nodes in group  $a$  by  $\pi_a$ , one obtains the estimation of  $Z_i$  as

$$Z_i \approx \sum_{a=1}^q \pi_a \exp \left\{ \mathbf{x}_i^T \boldsymbol{\mu}_a + \frac{1}{2} \mathbf{x}_i^T \Omega_a \mathbf{x}_i \right\} .$$

Coming to the algorithm's computational complexity, given that our choice of  $P$  is the sum of matrix products, the algorithm can be deployed in two forms: one in which  $P$  is never formally computed and the sequence  $\{\hat{L}_t\}_{t=1, \dots, T}$  is fed to the algorithm; and one in which  $P$  is explicitly computed. Letting  $X \in \mathbb{R}^{n \times d}$  be the matrix storing the embedding vectors in its rows, the computational complexity is determined by the matrix product  $PX$  needed to obtain the gradient of  $\mathcal{L}$ . In the former case, this is computed in  $\mathcal{O}(nd^2 + dE)$  operations, where  $E = \sum_{t=1}^T |\mathcal{E}_t|$  is the number of temporal edges. In the second case, instead, the complexity is given by the number of non-zero entries of  $P$ , which cannot exceed  $n^2$ . The former implementation is particularly convenient when  $n$  is large, and the  $\hat{L}_t$  matrices are very sparse. This is because  $P$  may be dense, even if the snapshots are sparse, and for large  $n$ ,  $P$  might not even fit in the computer's memory. Conversely, for small graphs,  $n^2$  may be smaller than the number of temporal edges, making the latter implementation more convenient.

## Matched distance definition

From (3), we have

$$\begin{aligned} d_m^2(X, Y) &= \sum_{i, j \in \mathcal{V}} [(M_X)_{ij} - (M_Y)_{ij}]^2 \\ &= \sum_{i, j \in \mathcal{V}} [(M_X)_{ij}(M_X)_{ij} + (M_Y)_{ij}(M_Y)_{ij} - 2(M_X)_{ij}(M_Y)_{ij}] \\ &\stackrel{(a)}{=} \sum_{i, j \in \mathcal{V}} [(M_X)_{ij}(M_X)_{ji} + (M_Y)_{ij}(M_Y)_{ji} - 2(M_X)_{ij}(M_Y)_{ji}] \\ &= \sum_{i \in \mathcal{V}} [(M_X M_X^T)_{ii} + (M_Y M_Y^T)_{ii} - 2(M_X M_Y^T)_{ii}] \\ &= \text{tr}(M_X M_X^T) + \text{tr}(M_Y M_Y^T) - 2\text{tr}(M_X M_Y^T) \\ &\stackrel{(b)}{=} \text{tr}(X X^T X X^T) + \text{tr}(Y Y^T Y Y^T) - 2\text{tr}(X X^T Y Y^T) \\ &\stackrel{(c)}{=} \text{tr}(X^T X X^T X) + \text{tr}(Y^T Y Y^T Y) - 2\text{tr}(Y^T X X^T Y) \\ &\stackrel{(d)}{=} \|X^T X\|_{\mathbb{F}}^2 + \|Y^T Y\|_{\mathbb{F}}^2 - 2\|X^T Y\|_{\mathbb{F}}^2, \end{aligned}$$

where in (a) we exploited that  $M_X$  and  $M_Y$  are symmetric, in (b) we used the definition of  $M_X, M_Y$ , in (c) we used that property of the trace stating that  $\text{tr}(AB) = \text{tr}(BA)$ , and finally in (d) we applied the definition of the Frobenius norm.

## Properties of the unmatched distance

In this section, we show that the unmatched distance is invariant with respect to node permutations, and, more generally, to any orthogonal transformation applied to the columns of the embedding matrix. We then show that the unmatched distance is also invariant with respect to any orthogonal transformation applied to the rows of the embedding matrix. This is necessary because the **EDRep** loss function is invariant under this type of transformation.

We consider a bijective node mapping  $\pi : \mathcal{V} \rightarrow \mathcal{V}$ . We let  $Q \in \mathbb{R}^{n \times n}$  be the permutation matrix defined as  $Q_{ij} = \delta_{j, \pi(i)}$ . In the matrix multiplication,  $Q$  swaps the entry  $i$  with  $\pi(i)$ :

$$\bar{X}_{ia} := (QX)_{ia} = \sum_{j \in \mathcal{V}} Q_{ij} X_{ja} = \sum_{j \in \mathcal{V}} \delta_{j, \pi(i)} X_{ja} = X_{\pi(i), a}.$$

The matrix  $Q$  is orthogonal, in fact

$$(QQ^T)_{ij} = \sum_{k \in \mathcal{V}} Q_{ik} Q_{jk} = \sum_{k \in \mathcal{V}} \delta_{k, \pi(i)} \delta_{k, \pi(j)} = \delta_{\pi(i), \pi(j)} = \delta_{ij},$$

where the last equality follows from  $\pi$  being a bijective mapping. As a consequence,  $QQ^T = Q^T Q = I_n$ . The distance  $d_u$  depends on the embedding matrix  $X$  only through  $X^T X$ . We now show that this expression is invariant under node permutation of the embedding matrix, or any orthogonal matrix  $Q$ . Indeed, let  $\bar{X} = QX$ , then

$$\bar{X}^T \bar{X} = X^T \underbrace{Q^T Q}_{I_n} X = X^T X.$$

We now show that the distance  $d_u$  is also invariant under the orthogonal transformation applied to the embedding matrix rows. Let  $R \in \mathbb{R}^{d \times d}$  be an orthogonal matrix and let  $\tilde{X} = XR$ . Letting  $\lambda_i(M)$  be the  $i$ -th smallest eigenvalue of  $M$ , then, for all  $i$ ,  $\lambda_i(AB) = \lambda_i(BA)$  [82, Theorem 1.3.22]. It follows

$$\lambda_i(\tilde{X}^T \tilde{X}) = \lambda_i(R^T X^T X R) = \lambda_i(\underbrace{R R^T}_{I_d} X^T X) = \lambda_i(X^T X),$$

thus proving the claim.

## Temporal graph randomizations

In Table 1 we summarize the properties of the temporal graphs we used to conduct our tests.

We now give a more detailed description of the randomization techniques we adopted, defined in terms of the quantities they preserve. According to the method, it may be more convenient to represent the temporal graph as a sequence of instantaneous interactions  $(i, j, t)$ , as a sequence of interactions with a duration  $(i, j, t, \tau)$ , or as a sequence of weighted adjacency matrices  $W^{(t)}$  [69]. Before randomization, time is discretized at the scale of 10 minutes in each data set, and the cumulative interaction time in each 10-minute window is used as weight.

1. *Random.* Temporal edges are represented as  $(i, j, t)$  and all three indices are randomized, avoiding self-edges ( $i$  and  $j$  randomized between 1 and  $n$ , and  $t$  between 1 and  $T$ ).  
**Preserved quantities:** number of temporal edges.
2. *Random delta.* Temporal edges are represented as  $(i, j, t, \tau)$ . Once again,  $i, j, t$  are randomized ( $t$  is sampled between 1 and  $T - \tau$ ), while  $\tau$  is preserved.  
**Preserved quantities:** number of temporal edges and interaction duration distribution.
3. *Active snapshot.* At each time step  $t$ , the edges are randomly replaced between active nodes at  $t$ , *i.e.* that had at least one neighbor in the original snapshot.  
**Preserved quantities:** number of edges at each time-step and activity pattern of each node.

Table 1: Summary properties of the **SocioPatterns** time-resolved proximity networks used here. *Graph name* is used to identify the graphs; *Description* provides concise information on the context where data were collected;  $n$  is the number of graph nodes; *Duration* is the temporal span of the data set, and  $T$  is the number of graph snapshots.

Graph name	Description	$n$	Duration	$T$
<i>Primary school</i> [75, 83]	Children of 10 classes of a primary school	242	2 days	194
<i>High school 1</i> [84]	Students of 3 classes of a high school in 2011	126	4 days	453
<i>High school 2</i> [84]	Students of 5 classes of a high school in 2012	180	7 days	1215
<i>High school 3</i> [85]	Students of 9 classes of a high school in 2013	327	5 days	605
<i>Baboons</i> [86]	A group of baboons	13	27 days	3986
<i>Households</i> [87]	People of a village in Malawi	86	26 days	1926
<i>Hospital</i> [88]	Patients and health-care workers of a hospital	75	5 days	579
<i>Conference</i> [13]	People at a medical conference	405	2 days	190
<i>Office</i> [89]	Office workers in an office building	92	19 days	1646

4. *Time*. Temporal edges are represented as  $(i, j, t)$  and only the index  $t$  is randomized.  
**Preserved quantities:** aggregated graph structure.
5. *Sequence*. The graph is represented as a sequence of weighted adjacency matrices  $W^{(t)}$  and the randomization acts on the indices  $t$ .  
**Preserved quantities:** the structure of each snapshot.
6. *Weighted degree*. Temporal edges are represented as  $(i, j, t)$  and all three indices are randomized as in *Random* but with the constraint that each node appears in the same number of temporal edges as in the original network.  
**Preserved quantities:** nodes weighted degree.

## Synthetic models

We here provide a formal definition of the models used to generate the synthetic graphs under analysis. Even though we considered four models, three of these can be generated from the *degree corrected stochastic block model* [63] by changing its parameters.

**Definition 3 (Degree corrected stochastic block model)** Let  $\mathcal{V}$  be a set of  $n$  nodes and  $\ell \in [k]^n$  be a vector mapping each node to a class. Further let  $C \in \mathbb{R}^{k \times k}$  be a positive symmetric matrix and  $\theta \in \mathbb{R}^n$  be a vector satisfying  $\theta^T \mathbf{1}_n = n$ . The entries of the graph adjacency matrix  $A \in [0, 1]^{n \times n}$  are generated independently (up to symmetry) at random with probability

$$\mathbb{P}(A_{ij} = 1) = \min \left( 1, \theta_i \theta_j \frac{C_{\ell_i, \ell_j}}{n} \right).$$

The vector  $\ell$  contains the labels and gives a community structure in the case in which  $C_{a,a} > C_{a,b}$  for  $b \neq a$ , meaning that there is a higher probability that two nodes in the same community will get connected.



The value  $\theta_i$  is proportional to the expected degree of node  $i$ . For this reason, if one chooses  $\boldsymbol{\theta} = \mathbf{1}_n$  and  $\boldsymbol{\ell} = \mathbf{1}_n$ , one gets the Erdős-Renyi model, in which every node has the same expected degree, and there are no communities. The configuration model, instead, is obtained by letting  $\boldsymbol{\ell} = \mathbf{1}_n$ , but changing the value of  $\boldsymbol{\theta}$  to create an arbitrary degree distribution that we choose to be a (properly rescaled) uniform distribution between 3 and 10 raised to the power 4. Finally, the stochastic block model is obtained from a labeling vector different from  $\mathbf{1}_n$  and letting  $\boldsymbol{\theta} = \mathbf{1}_n$ . We consider  $k = 5$  communities of equal size with  $C_{a,b} = 20\delta_{ab} + (1 - \delta_{ab})$ , with  $\delta$  the Kroeneker symbol.

Let us finally introduce the random geometric model.

**Definition 4 (Random geometric model)** *Let  $\mathcal{V}$  be a set of  $n$  nodes. For each  $i \in \mathcal{V}$  let  $\mathbf{x}_i \in \mathbb{R}^2$  be a random vector with norm  $\|\mathbf{x}_i\| \leq 1$ . The entries of the graph adjacency matrix  $A \in [0, 1]^{n \times n}$  are generated independently (up to symmetry) at random with probability*

$$\mathbb{P}(A_{ij} = 1) = e^{-\beta \|\mathbf{x}_i - \mathbf{x}_j\|},$$

for some positive  $\beta$ .

Note that even though the entries of  $A$  are drawn at random, this model can generate graphs with a high clustering coefficient because the probability depends on the relative distance of a fixed embedding. In our simulations, we set  $\beta = 20$ .

## Acknowledgments

LD and CC acknowledge support from the Lagrange Project of the ISI Foundation funded by CRT Foundation and from Fondation Botnar (EPFL COVID-19 Real Time Epidemiology I-DAIR Pathfinder). AB acknowledges support from the Agence Nationale de la Recherche (ANR) project DATAREDEX (ANR-19-CE46-0008).

## Authors contributions

LD formalized the research problem, developed computer code, carried out the analysis, and wrote the first version of the manuscript. All authors contributed to framing the research questions, discussing the results, and writing the manuscript.

## Data availability

All data used in this article are publicly available at <http://www.sociopatterns.org/datasets/>.

## Code availability

Commented Python code to reproduce our results is available at [github.com/lorenzodallamico/G-DynaDist](https://github.com/lorenzodallamico/G-DynaDist).

## Competing interests

The authors do not declare any competing interests.

## References

- [1] Albert-László Barabási and Réka Albert. Emergence of scaling in random networks. *science*, 286(5439):509–512, 1999.

- [2] Mark EJ Newman. The structure and function of complex networks. *SIAM review*, 45(2):167–256, 2003.
- [3] A. Barrat, M. Barthélemy, and A. Vespignani. *Dynamical processes on complex networks*. Cambridge University Press, Cambridge, 2008.
- [4] John Scott. Trend report social network analysis. *Sociology*, pages 109–127, 1988.
- [5] Stanley Wasserman and Katherine Faust. *Social Network Analysis: Methods and Applications*. Structural Analysis in the Social Sciences. Cambridge University Press, 1994.
- [6] Luis A Nunes Amaral, Antonio Scala, Marc Barthelemy, and H Eugene Stanley. Classes of small-world networks. *Proceedings of the national academy of sciences*, 97(21):11149–11152, 2000.
- [7] Marc Barthélemy. Spatial networks. *Physics reports*, 499(1-3):1–101, 2011.
- [8] Eric Alm and Adam P Arkin. Biological networks. *Current opinion in structural biology*, 13(2):193–202, 2003.
- [9] Petter Holme and Jari Saramäki. Temporal networks. *Physics reports*, 519(3):97–125, 2012.
- [10] Ling Zhao, Yujiao Song, Chao Zhang, Yu Liu, Pu Wang, Tao Lin, Min Deng, and Haifeng Li. T-gcn: A temporal graph convolutional network for traffic prediction. *IEEE transactions on intelligent transportation systems*, 21(9):3848–3858, 2019.
- [11] Benjamin Blonder, Tina W Wey, Anna Dornhaus, Richard James, and Andrew Sih. Temporal dynamics and network analysis. *Methods in Ecology and Evolution*, 3(6):958–972, 2012.
- [12] Nathan Eagle, Alex Pentland, and David Lazer. Inferring friendship network structure by using mobile phone data. *Proceedings of the national academy of sciences*, 106(36):15274–15278, 2009.
- [13] Ciro Cattuto, Wouter Van den Broeck, Alain Barrat, Vittoria Colizza, Jean-François Pinton, and Alessandro Vespignani. Dynamics of person-to-person interactions from distributed rfid sensor networks. *PloS one*, 5(7):e11596, 2010.
- [14] Alain Barrat, Ciro Cattuto, Vittoria Colizza, Francesco Gesualdo, Lorenzo Isella, Elisabetta Pandolfi, J-F Pinton, Lucilla Ravà, Caterina Rizzo, Mariateresa Romano, et al. Empirical temporal networks of face-to-face human interactions. *The European Physical Journal Special Topics*, 222(6):1295–1309, 2013.
- [15] Alain Barrat and Ciro Cattuto. Temporal networks of face-to-face human interactions. In *Temporal Networks*, pages 191–216. Springer, 2013.
- [16] Arkadiusz Stopczynski, Vedran Sekara, Piotr Sapiezynski, Andrea Cuttone, Mette My Madsen, Jakob Eg Larsen, and Sune Lehmann. Measuring large-scale social networks with high resolution. *PloS one*, 9(4):e95978, 2014.
- [17] Gecia Bravo-Hermesdorff, Valkyrie Felso, Emily Ray, Lee M Gunderson, Mary E Helander, Joana Maria, and Yael Niv. Gender and collaboration patterns in a temporal scientific authorship network. *Applied Network Science*, 4(1):1–17, 2019.
- [18] Remy Cazabet, Pablo Jensen, and Pierre Borgnat. Tracking the evolution of temporal patterns of usage in bicycle-sharing systems using nonnegative matrix factorization on multiple sliding windows. *International Journal of Urban Sciences*, 22(2):147–161, 2018.
- [19] Trine Agervig Carstensen, Anton Stahl Olafsson, Nynne Marie Bech, Thea Schmidt Poulsen, and Chunli Zhao. The spatio-temporal development of copenhagen’s bicycle infrastructure 1912–2013. *Geografisk Tidsskrift-Danish Journal of Geography*, 115(2):142–156, 2015.
- [20] Aurélien Bellet, Amaury Habrard, and Marc Sebban. Metric learning. *Synthesis lectures on artificial intelligence and machine learning*, 9(1):1–151, 2015.

- [21] Peter Wills and François G Meyer. Metrics for graph comparison: a practitioner’s guide. *Plos one*, 15(2):e0228728, 2020.
- [22] Mattia Tantardini, Francesca Ieva, Lucia Tajoli, and Carlo Piccardi. Comparing methods for comparing networks. *Scientific reports*, 9(1):1–19, 2019.
- [23] Hartle Harrison, Klein Brennan, McCabe Stefan, Daniels Alexander, St-Onge Guillaume, Murphy Charles, and Hébert-Dufresne Laurent. Network comparison and the within-ensemble graph distance. *Proc. R. Soc. A*, 476:20190744, 2020.
- [24] Claudio DT Barros, Matheus RF Mendonça, Alex B Vieira, and Artur Ziviani. A survey on embedding dynamic graphs. *ACM Computing Surveys (CSUR)*, 55(1):1–37, 2021.
- [25] Guixiang Ma, Nesreen K Ahmed, Theodore L Willke, and Philip S Yu. Deep graph similarity learning: A survey. *Data Mining and Knowledge Discovery*, 35(3):688–725, 2021.
- [26] Alberto Sanfeliu and King-Sun Fu. A distance measure between attributed relational graphs for pattern recognition. *IEEE transactions on systems, man, and cybernetics*, (3):353–362, 1983.
- [27] Danai Koutra, Joshua T Vogelstein, and Christos Faloutsos. Deltacon: A principled massive-graph similarity function. In *Proceedings of the 2013 SIAM international conference on data mining*, pages 162–170. SIAM, 2013.
- [28] Nathan D Monnig and François G Meyer. The resistance perturbation distance: A metric for the analysis of dynamic networks. *Discrete Applied Mathematics*, 236:347–386, 2018.
- [29] Michele Berlingerio, Danai Koutra, Tina Eliassi-Rad, and Christos Faloutsos. Netsimile: A scalable approach to size-independent network similarity. *arXiv preprint arXiv:1209.2684*, 2012.
- [30] James P Bagrow and Erik M Bollt. An information-theoretic, all-scales approach to comparing networks. *Applied Network Science*, 4(1):1–15, 2019.
- [31] Neural Nets WIRN10 B Apolloni et al. An introduction to spectral distances in networks. In *Neural Nets WIRN10: Proceedings of the 20th Italian Workshop on Neural Nets*, volume 226, page 227. IOS Press, 2011.
- [32] Yutaka Shimada, Yoshito Hirata, Tohru Ikeguchi, and Kazuyuki Aihara. Graph distance for complex networks. *Scientific reports*, 6(1):1–6, 2016.
- [33] Leo Torres, Pablo Suarez-Serrato, and Tina Eliassi-Rad. Graph distance from the topological view of non-backtracking cycles. *arXiv preprint arXiv:1807.09592*, 2018.
- [34] Anton Tsitsulin, Davide Mottin, Panagiotis Karras, Alexander Bronstein, and Emmanuel Müller. Netlsd: hearing the shape of a graph. In *Proceedings of the 24th ACM SIGKDD International Conference on Knowledge Discovery & Data Mining*, pages 2347–2356, 2018.
- [35] Claire Donnat and Susan Holmes. Tracking network dynamics: A survey using graph distances. *The Annals of Applied Statistics*, 12(2):971–1012, 2018.
- [36] Naoki Masuda and Petter Holme. Detecting sequences of system states in temporal networks. *Scientific reports*, 9(1):1–11, 2019.
- [37] Valeria Gelardi, Joël Fagot, Alain Barrat, and Nicolas Claidière. Detecting social (in) stability in primates from their temporal co-presence network. *Animal Behaviour*, 157:239–254, 2019.
- [38] Nicola Pedreschi, Christophe Bernard, Wesley Clawson, Pascale Quilichini, Alain Barrat, and Demian Battaglia. Dynamic core-periphery structure of information sharing networks in entorhinal cortex and hippocampus. *Network Neuroscience*, 4(3):946–975, 2020.

- [39] Moran Beladev, Lior Rokach, Gilad Katz, Ido Guy, and Kira Radinsky. *tdgraphembed: Temporal dynamic graph-level embedding*. In *Proceedings of the 29th ACM International Conference on Information & Knowledge Management*, pages 55–64, 2020.
- [40] Chenghan Huang, Lili Wang, Xinyuan Cao, Weicheng Ma, and Soroush Vosoughi. Learning dynamic graph embeddings using random walk with temporal backtracking. In *NeurIPS 2022 Temporal Graph Learning Workshop*, 2022.
- [41] Didier Le Bail, Mathieu Génois, and Alain Barrat. Flow of temporal network properties under local aggregation and time shuffling: a tool for characterizing, comparing and classifying temporal networks. *arXiv preprint arXiv:2310.09112*, 2023.
- [42] Vincent Froese, Brijnesh Jain, Rolf Niedermeier, and Malte Renken. Comparing temporal graphs using dynamic time warping. *Social Network Analysis and Mining*, 10(1):1–16, 2020.
- [43] Xiu-Xiu Zhan, Chuang Liu, Zhipeng Wang, Huijuang Wang, Petter Holme, and Zi-Ke Zhang. Measuring and utilizing temporal network dissimilarity. *arXiv preprint arXiv:2111.01334*, 2021.
- [44] Giulio Rossetti and Rémy Cazabet. Community discovery in dynamic networks: a survey. *ACM computing surveys (CSUR)*, 51(2):1–37, 2018.
- [45] Mikhael Gromov, Misha Katz, Pierre Pansu, and Stephen Semmes. *Metric structures for Riemannian and non-Riemannian spaces*, volume 152. Springer, 1999.
- [46] Hongyun Cai, Vincent W Zheng, and Kevin Chen-Chuan Chang. A comprehensive survey of graph embedding: Problems, techniques, and applications. *IEEE Transactions on Knowledge and Data Engineering*, 30(9):1616–1637, 2018.
- [47] Palash Goyal and Emilio Ferrara. Graph embedding techniques, applications, and performance: A survey. *Knowledge-Based Systems*, 151:78–94, 2018.
- [48] Mengjia Xu. Understanding graph embedding methods and their applications. *SIAM Review*, 63(4):825–853, 2021.
- [49] Ilya Makarov, Dmitrii Kiselev, Nikita Nikitinsky, and Lovro Subelj. Survey on graph embeddings and their applications to machine learning problems on graphs. *PeerJ Computer Science*, 7:e357, 2021.
- [50] Laetitia Gauvin, André Panisson, and Ciro Cattuto. Detecting the community structure and activity patterns of temporal networks: a non-negative tensor factorization approach. *PloS one*, 9(1):e86028, 2014.
- [51] Yun Chi, Xiaodan Song, Dengyong Zhou, Koji Hino, and Belle L Tseng. Evolutionary spectral clustering by incorporating temporal smoothness. In *Proceedings of the 13th ACM SIGKDD international conference on Knowledge discovery and data mining*, pages 153–162, 2007.
- [52] Xuanmei Qin, Weidi Dai, Pengfei Jiao, Wenjun Wang, and Ning Yuan. A multi-similarity spectral clustering method for community detection in dynamic networks. *Scientific reports*, 6(1):1–11, 2016.
- [53] Fuchen Liu, David Choi, Lu Xie, and Kathryn Roeder. Global spectral clustering in dynamic networks. *Proceedings of the National Academy of Sciences*, 115(5):927–932, 2018.
- [54] Kevin S Xu, Mark Klinger, and Alfred O Hero III. Adaptive evolutionary clustering. *Data Mining and Knowledge Discovery*, 28(2):304–336, 2014.
- [55] Lorenzo Dall’Amico, Romain Couillet, and Nicolas Tremblay. Community detection in sparse time-evolving graphs with a dynamical bethe-hessian. *Advances in Neural Information Processing Systems*, 33:7486–7497, 2020.
- [56] Yuan Zuo, Guannan Liu, Hao Lin, Jia Guo, Xiaoqian Hu, and Junjie Wu. Embedding temporal network via neighborhood formation. In *Proceedings of the 24th ACM SIGKDD international conference on knowledge discovery & data mining*, pages 2857–2866, 2018.

- [57] Giang Hoang Nguyen, John Boaz Lee, Ryan A Rossi, Nesreen K Ahmed, Eunye Koh, and Sungchul Kim. Continuous-time dynamic network embeddings. In *Companion proceedings of the the web conference 2018*, pages 969–976, 2018.
- [58] Koya Sato, Mizuki Oka, Alain Barrat, and Ciro Cattuto. Predicting partially observed processes on temporal networks by dynamics-aware node embeddings (dyane). *EPJ Data Science*, 10(1):22, 2021.
- [59] Jari Saramäki and Petter Holme. Exploring temporal networks with greedy walks. *The European Physical Journal B*, 88:1–8, 2015.
- [60] Lorenzo Dall’Amico and Enrico Maria Belliardo. Efficient distributed representations beyond negative sampling. *arXiv preprint arXiv:2303.17475*, 2023.
- [61] Lorenzo Isella, Juliette Stehlé, Alain Barrat, Ciro Cattuto, Jean-François Pinton, and Wouter Van den Broeck. What’s in a crowd? analysis of face-to-face behavioral networks. *Journal of theoretical biology*, 271(1):166–180, 2011.
- [62] Paul Erdős, Alfréd Rényi, et al. On the evolution of random graphs. *Publ. math. inst. hung. acad. sci.*, 5(1):17–60, 1960.
- [63] Brian Karrer and Mark EJ Newman. Stochastic blockmodels and community structure in networks. *Physical review E*, 83(1):016107, 2011.
- [64] Béla Bollobás. A probabilistic proof of an asymptotic formula for the number of labelled regular graphs. *European Journal of Combinatorics*, 1(4):311–316, 1980.
- [65] Jesper Dall and Michael Christensen. Random geometric graphs. *Physical review E*, 66(1):016121, 2002.
- [66] Cédric Févotte and Jérôme Idier. Algorithms for nonnegative matrix factorization with the  $\beta$ -divergence. *Neural computation*, 23(9):2421–2456, 2011.
- [67] James MacQueen et al. Some methods for classification and analysis of multivariate observations. In *Proceedings of the fifth Berkeley symposium on mathematical statistics and probability*, volume 1, pages 281–297. Oakland, CA, USA, 1967.
- [68] Tim Sainburg, Leland McInnes, and Timothy Q Gentner. Parametric umap embeddings for representation and semisupervised learning. *Neural Computation*, 33(11):2881–2907, 2021.
- [69] Laetitia Gauvin, Mathieu Génois, Márton Karsai, Mikko Kivela, Taro Takaguchi, Eugenio Valdano, and Christian L Vestergaard. Randomized reference models for temporal networks. *SIAM Review*, 64(4):763–830, 2022.
- [70] Raj Kumar Pan and Jari Saramäki. Path lengths, correlations, and centrality in temporal networks. *Phys. Rev. E*, 84:016105, Jul 2011.
- [71] Ian Goodfellow, Jean Pouget-Abadie, Mehdi Mirza, Bing Xu, David Warde-Farley, Sherjil Ozair, Aaron Courville, and Yoshua Bengio. Generative adversarial nets. *Advances in neural information processing systems*, 27, 2014.
- [72] Faezeh Faez, Yassaman Ommi, Mahdiah Soleymani Baghshah, and Hamid R Rabiee. Deep graph generators: A survey. *IEEE Access*, 9:106675–106702, 2021.
- [73] Hamed Alqahtani, Manolya Kavakli-Thorne, and Gulshan Kumar. Applications of generative adversarial networks (gans): An updated review. *Archives of Computational Methods in Engineering*, 28:525–552, 2021.
- [74] Anna Machens, Francesco Gesualdo, Caterina Rizzo, Alberto E. Tozzi, Alain Barrat, and Ciro Cattuto. An infectious disease model on empirical networks of human contact: bridging the gap between dynamic network data and contact matrices. *BMC Infectious Diseases*, 13(1):1–18, 2013.



- [75] Valerio Gemmetto, Alain Barrat, and Ciro Cattuto. Mitigation of infectious disease at school: targeted class closure vs school closure. *BMC infectious diseases*, 14(1):1–10, 2014.
- [76] Dina Mistry, Maria Litvinova, Ana Pastore y Piontti, Matteo Chinazzi, Laura Fumanelli, Marcelo FC Gomes, Syed A Haque, Quan-Hui Liu, Kunpeng Mu, Xinyue Xiong, et al. Inferring high-resolution human mixing patterns for disease modeling. *Nature communications*, 12(1):323, 2021.
- [77] Giulia Cencetti, Gabriele Santin, Antonio Longa, Emanuele Pigani, Alain Barrat, Ciro Cattuto, Sune Lehmann, Marcel Salathe, and Bruno Lepri. Digital proximity tracing on empirical contact networks for pandemic control. *Nature communications*, 12(1):1655, 2021.
- [78] Ana-Maria Crețu, Federico Monti, Stefano Marrone, Xiaowen Dong, Michael Bronstein, and Yves-Alexandre de Montjoye. Interaction data are identifiable even across long periods of time. *Nature Communications*, 13(1):313, 2022.
- [79] Elisabetta Colosi, Giulia Bassignana, Diego Andrés Contreras, Canelle Poirier, Pierre-Yves Boëlle, Simon Cauchemez, Yazdan Yazdanpanah, Bruno Lina, Arnaud Fontanet, Alain Barrat, and Vittoria Colizza. Screening and vaccination against covid-19 to minimise school closure: a modelling study. *The Lancet Infectious Diseases*, 22(7):977–989, 2022.
- [80] Lars Backstrom, Cynthia Dwork, and Jon Kleinberg. Wherefore art thou r3579x? anonymized social networks, hidden patterns, and structural steganography. In *Proceedings of the 16th international conference on World Wide Web*, pages 181–190, 2007.
- [81] Daniele Romanini, Sune Lehmann, and Mikko Kivela. Privacy and uniqueness of neighborhoods in social networks. *Scientific reports*, 11(1):20104, 2021.
- [82] Roger A Horn and Charles R Johnson. *Matrix analysis*. Cambridge university press, 2012.
- [83] Juliette Stehlé, Nicolas Voirin, Alain Barrat, Ciro Cattuto, Lorenzo Isella, Jean-François Pinton, Marco Quaggiotto, Wouter Van den Broeck, Corinne Régis, Bruno Lina, et al. High-resolution measurements of face-to-face contact patterns in a primary school. *PloS one*, 6(8):e23176, 2011.
- [84] Julie Fournet and Alain Barrat. Contact patterns among high school students. *PLoS ONE*, 9(9):e107878, 09 2014.
- [85] Rossana Mastrandrea, Julie Fournet, and Alain Barrat. Contact patterns in a high school: a comparison between data collected using wearable sensors, contact diaries and friendship surveys. *PloS one*, 10(9):e0136497, 2015.
- [86] Valeria Gelardi, Jeanne Godard, Dany Paleressompouille, Nicolas Claidière, and Alain Barrat. Measuring social networks in primates: wearable sensors versus direct observations. *Proceedings of the Royal Society A*, 476(2236):20190737, 2020.
- [87] Laura Ozella, Daniela Paolotti, Guilherme Lichand, Jorge P Rodríguez, Simon Haenni, John Phuka, Onicio B Leal-Neto, and Ciro Cattuto. Using wearable proximity sensors to characterize social contact patterns in a village of rural malawi. *EPJ Data Science*, 10(1):46, 2021.
- [88] Philippe Vanhems, Alain Barrat, Ciro Cattuto, Jean-Francois Pinton, Nagham Khanafer, Corinne Regis, Byeul-a Kim, Brigitte Comte, and Nicolas Voirin. Estimating potential infection transmission routes in hospital wards using wearable proximity sensors. *PLoS ONE*, 8:e73970, 09 2013.
- [89] Mathieu Génois and Alain Barrat. Can co-location be used as a proxy for face-to-face contacts? *EPJ Data Science*, 7(1):1–18, 2018.